1	
2	Effect of Ultrasound Amplitude and Frequency
3	on Nanoparticle Diffusion in an Agarose Hydrogel
4	
5	
6	Alina Karki ¹ , Jeffrey S. Marshall ² and Junru Wu ¹
7	
8	¹ Department of Physics
9	² Department of Mechanical Engineering
10	The University of Vermont
11	Burlington, Vermont, U.S.A.
12	
13	
14	Corresponding Author: Jeffrey Marshall, Department of Mechanical Engineering, The
15	University of Vermont, Burlington, VT 05405, U.S.A. PHONE: 1 (802) 656-3826, EMAIL:
16	jmarsha1@uvm.edu.
17	
18	Keywords: biofilms, oscillating diffusion, nanoparticles, ultrasound
19	Running title: Acoustic enhancement of diffusion in a hydrogel

20 ABSTRACT

Exposure of nanoparticles in a porous medium, such as a hydrogel, to low-intensity ultrasound has been observed to dramatically enhance particle penetration rate. Enhancement of nanoparticle penetration is a key issue affecting applications such as biofilm mitigation and targeted drug delivery in human tissue. The current study used fluorescent imaging to obtain detailed experimental measurements of the effect of ultrasound amplitude and frequency on diffusion of nanoparticles of different diameters in an agarose hydrogel, which is often used as a simulant for biofilms and biological tissues. We demonstrate that the acoustic enhancement occurs via the phenomenon of oscillatory diffusion, in which a combination of an oscillatory flow together with random hindering of the particles by interaction with hydrogel proteins induces a stochastic random walk of the particles. The measured variation of acoustic diffusion coefficients with amplitude and frequency were used to validate a previous statistical theory of oscillatory diffusion based on the continuous time random walk approach.

I. INTRODUCTION

34

35

36

37

38

39

40

41

42

43

44

45

46

47

48

49

50

51

52

53

54

55

56

Most microorganisms have the capability to live in either a freely floating (planktonic) state or in a wall-bounded state called a biofilm, in which they are encapsulated by a hydrogel formed of proteins called extracellular polymeric substances (EPS). Bacteria, for instance, spend on average about 90% of their time in biofilms and the remaining 10% in a planktonic state. The EPS found in bacterial biofilms offer protection to the bacteria in a variety of ways, including shielding the bacteria from predators, reducing shear stress from fluid flows, and neutralizing antibiotic chemicals that are harmful to the bacteria (Singh et al., 2017). Bacterial biofilms pose a danger in promoting infectious diseases (Costerton et al., 1999), in contamination of water purification systems (particularly in restricted environments such as during space travel) (Makris et al., 2014; Venkateswaran et al., 2014; Singh et al., 2018), and in fouling water flow lines (Characklis, 1981), to name only a few important applications. A primary method for mitigation of biofilms is by transport of anti-microbial agents (called biocides) into the biofilm via nanoparticles (Han et al., 2017). Nanoparticle-based biofilm mitigation strategies include silver nanoparticles (Siddique et al., 2020), liposomes or lipid-polymer hybrid nanoparticles encapsulating antibiotic chemicals (Cheow et al., 2011; Forier et al., 2014; Ma et al., 2015), hybrid nanoparticles with antimicrobial polymeric surface coatings (Galvão et al., 2018), photothermal bacterial mitigation using gold nanoparticles heated by infrared light (Millenbaugh et al., 2015; Zharov et al., 2006), and magnetic iron-oxide nanoparticles (Li et al., 2019; Mohammed et al., 2017).

A key step in nanoparticle-based biofilm mitigation approaches involves forcing the nanoparticles to penetrate into the biofilm. For magnetic particles, penetration into the biofilm can be readily controlled by application of an external magnetic field (Li et al., 2017). Biofilm

penetration for liposomes is generally controlled by diffusion of the nanoparticles through the EPS matrix, which depending on the particle size relative to the pore size, can be influenced by a variety of hindering processes involving nanoparticle capture by the porous structure (Fatin-Rouge et al., 2004; Peulen and Wilkinson, 2011).

A number of investigators have observed that acoustic excitation can significantly enhance particle penetration into porous media. Thomas and Chrysikopoulos (2006) conducted experiments on acoustic enhancement of diffusion of particles in a packed bed of spheres, building on previous work by Vogler and Chrysikopoulos (2002) for acoustic enhancement of solute transport. These authors proposed a phenomenological model in which an effective acoustic diffusion coefficient was added to the molecular diffusion coefficient, where the acoustic diffusion coefficient is a function of the acoustic wave amplitude.

In studies of the effect of ultrasound on use of liposomes containing recombinant tissue plasminogen activator (tPA) for lytic treatment of acute stroke, Tiukinhoy-Laing et al. (2006) and Shaw et al. (2009) observed that exposing the liposomes to low-intensity ultrasound (120 kHz frequency) significantly helped to improve effectiveness of the treatment. However, the mechanism by which this improvement was achieved was not clearly identified in these papers. Schroeder et al. (2009) discussed the use of ultrasound to control release of drugs from liposomes for medical treatments.

Ma et al. (2015) conducted a study of antibiotic-containing liposome treatment of an alginate biofilm and reported that application of low intensity ultrasound significantly enhanced transport of liposomes into an alginate hydrogel, including both the liposome transport from solution to the hydrogel outer surface and liposome penetration into the hydrogel. Alginate and agarose hydrogels are often used as physical models for biofilms since they share similar

mechanical properties to the biofilm EPS, but they have the advantages of fast setup and consistent properties compared to natural biofilms (Jung et al., 2015; Rowley et al., 1990; Smidsrød et al., 1990). In a follow-up work, Ma et al. (2018) conducted a preliminary study of the effect of ultrasound on nanoparticle diffusion in a two-layer agarose hydrogel, in which the top layer is initially seeded with fluorescent nanoparticles and the bottom layer is unseeded. Using a single ultrasound frequency and amplitude and two different nanoparticle sizes, this work was the first to measure the enhancement of nanoparticle diffusion coefficient in a hydrogel caused by exposure to low-intensity ultrasound. These measurements were performed by fitting numerical solutions of the advection-diffusion equation with two adjustable coefficients - the diffusion coefficient and the acoustic streaming velocity - to the experimental nanoparticle concentration data.

Mathematical modeling of oscillatory diffusion dates back to statistical modeling using a two-time continuous time random walk theory (CTRW) by Balakrishnan and Venkataraman (1981), in which particles are assumed to randomly flip between an oscillating state and a state in which they move at a constant random walk velocity. A simple stochastic model for oscillatory diffusion was proposed by Marshall (2016) in which particles are again assumed to exist in one of two states -- either an oscillating state or a captured state, in which their motion is temporarily hindered by the surrounding porous medium. While the parameters used in this model did not relate clearly to the particle and porous medium physical parameters (such as particle diameter and pore size), the model demonstrates that the combination of free oscillation and random hindering results in a diffusive process, which in the limit of many particles can in fact be accurately modeled using the standard diffusion equation with an effective diffusion coefficient that depends on the amplitude of the oscillatory flow.

An experimental and modeling study was reported by Marshall et al. (2021) in which motion of individual particles was tracked in a packed bed of spherical beads subject to an oscillating flow field. The particle diffusive motion was found to be consistent with theoretical predictions for random walk processes, including linear variation of variance with time, power law variation of the power spectrum with inverse square of frequency, linear decrease of the autocorrelation function, and value of the ratio of kurtosis to variance squared close to 3. The experimental observations were used to propose a physics-based stochastic model for oscillatory diffusion which was shown to agree well with experimental predictions. Curran and Marshall (2021) reported a parametric study of this stochastic model, including good agreement with the analytical expression for effective diffusion coefficient obtained from the CTRW theory of Balakrishnan and Venkataraman (1981) within parameter ranges for which both the CTRW theory and the stochastic model assumptions are satisfied.

In the current paper, we conduct a detailed experimental study of the problem of acoustically-enhanced nanoparticle diffusion in a two-layer agarose hydrogel. The study extends and improves upon the work of Ma et al (2018), but uses a similar experimental set-up. The current study specifically examines the effect of different ultrasound amplitudes and frequencies on nanoparticle diffusion in a two-layered agarose hydrogel, and compares the observed variation of diffusion coefficient with amplitude and frequency to the CTRW theoretical results of Balakrishnan and Venkataraman (1981). The study also improves accuracy of the methodology used by Ma et al. (2018) by applying the requirement of particle mass conservation in order to eliminate one fitting parameter (acoustic streaming), allowing us to make more accurate measurements of the nanoparticle diffusion coefficient.

The experimental method used in the study is described in Section 2. Results of the ultrasound exposure on nanoparticle diffusion is described in Section 3, and discussion of results is given in Section 4.

II. EXPERIMENTAL METHOD

A. Hydrogel preparation

A two-layered 0.8% agarose hydrogel sample was prepared in a Petri dish with one layer of clear agarose gel and another layer seeded with fluorospheres of 20, 40 or 100 nm diameter particles. The 0.8% agarose solution was prepared by mixing 0.2 g of agarose powder to 24.5 ml of deionized distilled water in a microwavable flask. The solution was microwaved for about 2 min at 700 W power by swirling the flask occasionally until the agarose was completely dissolved. A surfactant, 1 ml of 5% sodium dodecyl sulfate (SDS) (5 g per 100 ml), was added to the agarose solution while magnetically stirring the solution at 90°C for 3 min. This surfactant was important to eliminate particle agglomeration during formation of the seeded agarose layer.

An amount of 12 ml of this solution was poured carefully over the Petri dish to avoid any bubble formation and allowed to set for 5 min at room temperature (22°C) to form a layer of clear agarose gel. For the seeded layer, a specified amount of carboxylate-modified microspheres (ThermoFisher Scientific) (200 µl for 20 nm particles and 50 µl for 40 and 100 nm particles) was first processed in a vortex mixer for 10 s and then added to the remaining 10 ml of clear agarose solution while continuously mixing by magnetic stirrer for 3 min at 90°C. The solution was then poured over the clear agarose hydrogel layer, again avoiding any bubble formation, and allowed to gel for 5 min at 22°C to form the upper layer of agarose hydrogel seeded with fluorospheres. The nanoparticle volume concentration in the seeded layer after hydrogel

formation (at the start of the diffusion experiments) was equal to 0.000128, 0.000118, and 0.000079 for the 20, 40 and 100 nm particles, respectively. As discussed in Section 3, the 100 nm particles exhibited minimal diffusion, so only a limited number of results were obtained with these particles.

B. Ultrasound experiment

As shown in Figure 1, the ultrasound system consisted of non-focused transducers of two different center frequencies (Olympus NDT Inc., Waltham, MA), a function generator (Hewlett Packard 3314) to generate pulsed signals, and a power amplifier (ENI 240 RF, Rochester, NY) to drive the transducer to produce one-dimensional ultrasonic waves. The hydrogel samples were kept in deionized water and exposed to ultrasound for either 5 or 10 min, with the transducer held at 1 cm distance from the hydrogel surface to ensure that exposure occurs in the near-field region of the transducer. Experiments were conducted for frequencies of 0.50, 1.0 and 2.25 MHz at 10% duty cycle and ultrasound amplitudes of 0.10, 0.15 and 0.18 MPa, corresponding to a spatially-averaged and temporally-averaged intensity (I_{SATA}) of acoustic waves of 0.36, 0.82 and 1.18 W/cm², respectively. The active radius of the acoustic transducer was b = 0.95 cm, and the Rayleigh distance was $a_R = b^2 / \lambda \cong 3.0$, 6.0 and 13.5 cm for cases with frequencies of 0.50, 1.0 and 2.25 MHz, respectively. The I_{SATA} of acoustic waves were determined by using the radiation force method (Beissner, 1987), and amplitudes were then determined using the equation

$$I = p^2 / \rho C, \tag{1}$$

where I is the acoustic intensity, p is acoustic pressure, ρ is fluid density, and C is speed of sound in water. The measurements of intensity and pressure amplitudes were taken in distilled and degassed water at room temperature (20°C) at 1 cm from the transducer.

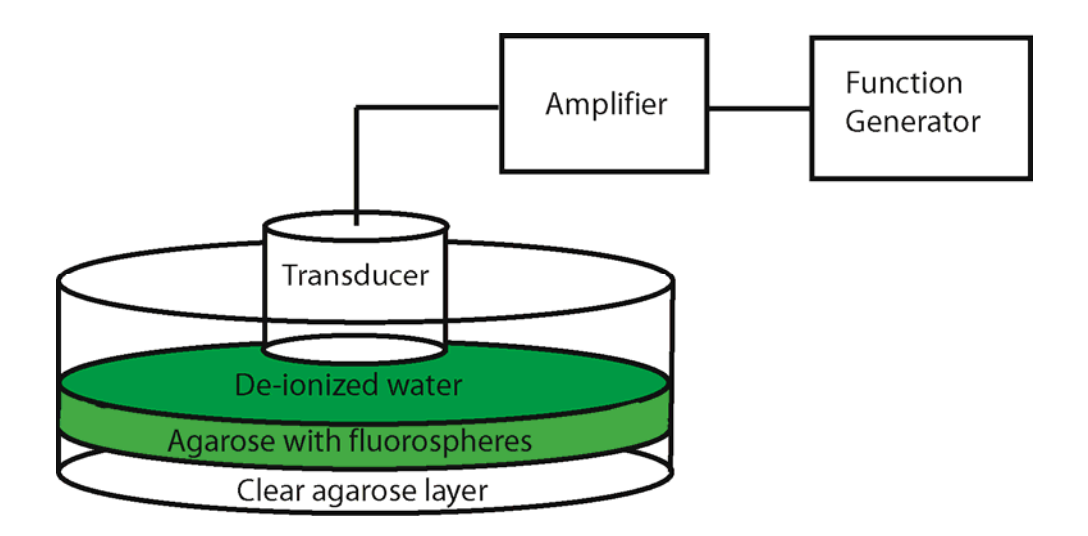


Figure 1. (Color online) Experimental set-up for the ultrasound measurements.

The transmission coefficient (T), ultrasound velocity, and attenuation coefficient of the hydrogel are listed for each transducer in Table I. These parameters were determined by measuring the transmitted signal through the two-layered hydrogel of thickness d = 2.1 mm using a hydrophone placed near the bottom of the clear agarose gel layer, using the equation

182
$$T = \frac{4Z_{w}Z_{h}}{[Z_{w} + Z_{h}]^{2}},$$
 (2)

where $Z_w = \rho_w C_w$ and $Z_h = \rho_h C_h$ are the acoustic impedances of water and hydrogel, respectively, and C_w and C_h are the ultrasound phase velocity in water and hydrogel. The

density of hydrogel was calculated as 0.98 ± 0.03 g/ml using the water displacement method (Dan-Asabe et al., 2013).

Table I. Data for ultrasound frequency (MHz), amplitude (MPa), transmission coefficient (*T*), speed of sound (m/s) and attenuation coefficient (dB/cm) used in the different experimental cases examined.

Frequency (MHz)	Amplitude (MPa)	Transmission coefficient	Speed of sound (m/s)	Attenuation coefficient (dB/cm)
1.00	0.10	0.999±0.003	1521±2.7	0.36±0.01
1.00	0.15	0.999±0.001	1521±8.7	0.41±0.01
1.00	0.18	0.998±0.015	1524±7.9	0.48±0.01
0.50	0.10	0.999±0.001	1516±12.5	0.56±0.01
2.25	0.10	0.995±0.009	1554±16.8	0.87±0.01

The hydrogel acoustic attenuation coefficient (α_h) for each transducer was calculated by comparing the log-magnitude of the ratio of the Fourier transform of the transmitted signal through the hydrogel sample (A_h) to that of a reference signal transmitted through distilled water (A_w) , such that (Wu, 1996)

$$\alpha_h = \frac{1}{d} \ln(TA_w / A_h). \tag{3}$$

Similarly, the ultrasound velocity was given by the phase velocity at the center frequency for each transducer. The ultrasound phase velocity in the hydrogel (C_h) was derived from the phase of the complex spectra, given by Wu (1996) as

$$C_{h} = C_{w} \left[1 + \frac{C_{w}(\phi_{h} - \phi_{w} \pm 2\pi m)}{2\pi f d} \right]^{-1}$$
(4)

where

$$\phi_h = \tan^{-1} \left[\frac{\operatorname{Im}(A_h)}{\operatorname{Re}(A_h)} \right], \qquad \phi_w = \tan^{-1} \left[\frac{\operatorname{Im}(A_w)}{\operatorname{Re}(A_w)} \right]$$
 (5)

are the phase angles of the amplitude spectra of the hydrogel and water, respectively. The term $\pm 2\pi m$ in (4) accounts for the ambiguity of the phase spectrum calculated from the arctangent function, where m is an integer.

The hydrogel was placed in a petri dish and immersed in the distilled water during the measurement. The transmission coefficient is inherent property of the material; hence it had no dependence on the frequency and amplitude. Uncertainty in the values recorded in Table I was determined by the root-mean square value of three repeated measurements. Over 99.5% of the incident ultrasound beam was transmitted through the hydrogel.

C. Imaging

A cross-section from the two-layer agarose hydrogel was used as a sample for the imaging using a Nikon A1R confocal microscope located at the University of Vermont Imaging Center. The samples were cut from the same Petri dish to test for different ultrasound conditions. The images obtained from the microscope depict the left-hand side as the initially seeded layer and the right-hand side as the initially clear layer, with the interface between them coinciding with the origin (x = 0), as shown in Figure 2a-d for different ultrasound amplitudes using 1 MHz ultrasound frequency with 20 nm particles. The fluorescence intensity line profile can be obtained from these images using NIS software, where it is assumed that the fluorescence F is

proportional to the particle concentration c. The experiments were repeated three times for each case, with three different agarose hydrogels, and tests for each condition were performed on the same day to maintain the same ambient environment. Five intensity line profiles were drawn from each image. The experimental mean and least-square values were obtained using these 5 intensity lines for each image.

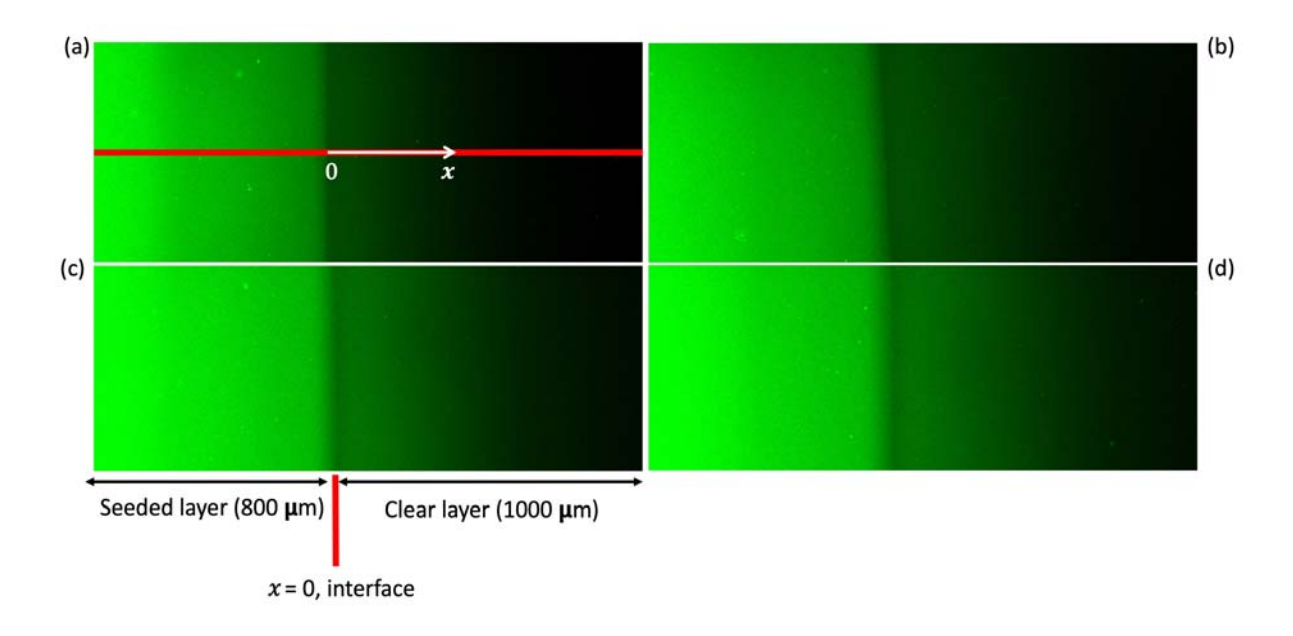


Figure 2. (Color online) Images obtained from a confocal microscope for the agarose hydrogel seeded with 20nm particles for different ultrasound conditions after 45 minutes of hydrogel formation: (a) control (no ultrasound); (b) treated using 1 MHz, 0.10 MPa ultrasound waves; (c) treated using 1 MHz, 0.15 MPa ultrasound waves; (d) treated using 1 MHz, 0.18 MPa ultrasound waves.

III. RESULTS

We are interested to study the diffusion process of different particle sizes in agarose hydrogel with and without treatment by ultrasound. Diffusion results are presented by plotting the normalized nanoparticle concentration $\hat{c} \equiv c/c_0$ as a function of the normalized distance into

the hydrogel $\hat{x} = x/L$. Here, c_0 is the value of particle concentration initially within the seeded layer and L=1 mm is the nominal length scale of the layer thickness. The value of \hat{c} was measured by averaging the fluorescence F(x,t) as a function of distance and time on five horizontal lines within an image (such as those in Figure 2) within a series of 100 bins along the x-axis. The maximum value of fluorescence was set equal to the maximum fluorescence F_0 , and the normalized concentration was estimated as $\hat{c} \cong F/F_0$. The origin was determined for each line by the requirement of nanoparticle mass conservation, which for a one-dimensional diffusion process requires that the integral under the concentration curve is conserved in time. This mass conservation condition also serves to subtract out from the data the effects of any small convective effects, such as might be caused by acoustic streaming within the hydrogel or motion driven by acoustic radiation pressure (King, 1934). The resulting concentration curves can therefore be fit by solution of the diffusion equation (as described in Section IV) using the diffusion coefficient as a single fitting parameter.

Diffusion results for each particle size for control cases (i.e., cases without ultrasound treatment) are shown in Figure 3a, with the imaging conducted 45 min after hydrogel formation. The curves shown were formed by connecting the average values of 100 bins using line segments. The rate of diffusion was found to increase as the particle size decreases. The 100 nm diameter particles exhibited very little diffusion, so we conclude that these particles must be either larger than, or at least approaching, the hydrogel pore size. Figure 3b shows diffusion results for the control case with 20 nm particles at times of 10, 20, 30 and 40 min after hydrogel formation. One measure of diffusion of particles from the initially seeded layer into the initially unseeded layer is obtained by integrating under the normalized concentration curve over the

interval $\hat{x} \in (0,1)$, corresponding to the initially unseeded layer, to yield the *integral penetration* measure P, defined by

$$P(t) = \int_{0}^{1} \hat{c}(\hat{x}, t) d\hat{x} . \tag{6}$$

For the case shown in Figure 3b, we obtained P = 0.0446, 0.0696, 0.0882 and 0.1087 for images at 10, 20, 30 and 40 min, respectively.

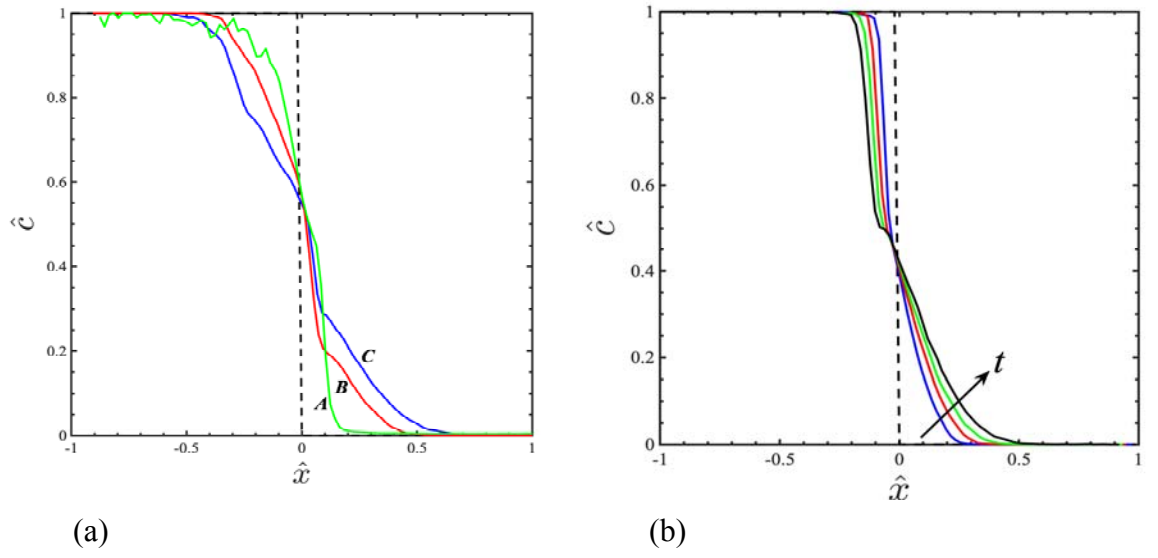


Figure 3. (Color online) Plots of particle normalized concentration \hat{c} as a function of dimensionless distance \hat{x} for control cases: (a) comparison at 45 min after hydrogel formation for particle diameters 20 nm (C, blue), 40 nm (B, red) and 100 nm (A, green); (b) plot for 20 nm particles at times after hydrogel formation of 10 min (blue), 20 min (red), 30 min (green) and 40 min (black). The standard deviation estimates lie within 0.01 for each condition. The arrow in (b) shows the direction of increasing time (t).

Experiments were conducted with different particle sizes and ultrasound amplitudes and frequencies, in which the particle fluorescence was measured at 45 min after gel formation.

Results obtained by varying ultrasound amplitude from 0.10-0.18 MPa for cases with 20nm

particles and ultrasound frequency 1 MHz frequency at 10% duty cycle and 5 min exposure are compared with the control case (with no ultrasound) in Figure 4a. It was generally observed that particle diffusion rate is enhanced by the application of ultrasound, with the amount of diffusion increasing as the ultrasound amplitude increases. The same tests conducted for 40 nm diameter particles are shown in Figure 4b, which similarly exhibits the trend of increasing particle diffusion rate with increase in ultrasound amplitude.

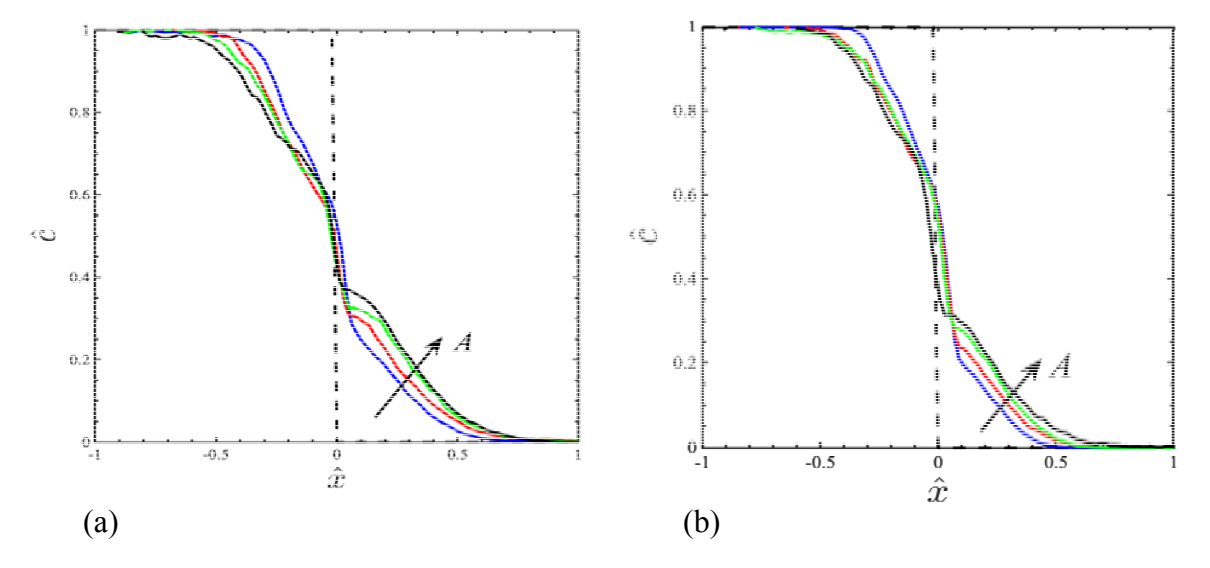


Figure 4. (Color online) Plots of normalized particle concentration for (a) 20 nm diameter particles and (b) 40nm particles measured at 45 min after hydrogel formation for the control case (blue) and cases treated with ultrasound of amplitude 0.10 MPa (red), 0.15 MPa (green) and 0.18 MPa (black) at 1 MHz frequency. The arrow shows the direction of increasing amplitude (4)

Figure 5 compares the control case with ultrasound-treated cases for frequencies of 0.50, 1.00 and 2.25 MHz, all with amplitude 0.10 MPa, 10% duty cycle and 5 min ultrasound exposure time. The results show a clear enhancement of particle diffusion rate due to the imposition of ultrasound. A comparison of the results obtained with the three frequencies were closer to each other than was the control case, and show a small enhancement of particle diffusion rate with

increase in ultrasound frequency. Results obtained with 20 nm particles (Figure 5a) and 40 nm particles (Figure 5b) exhibit similar trends.

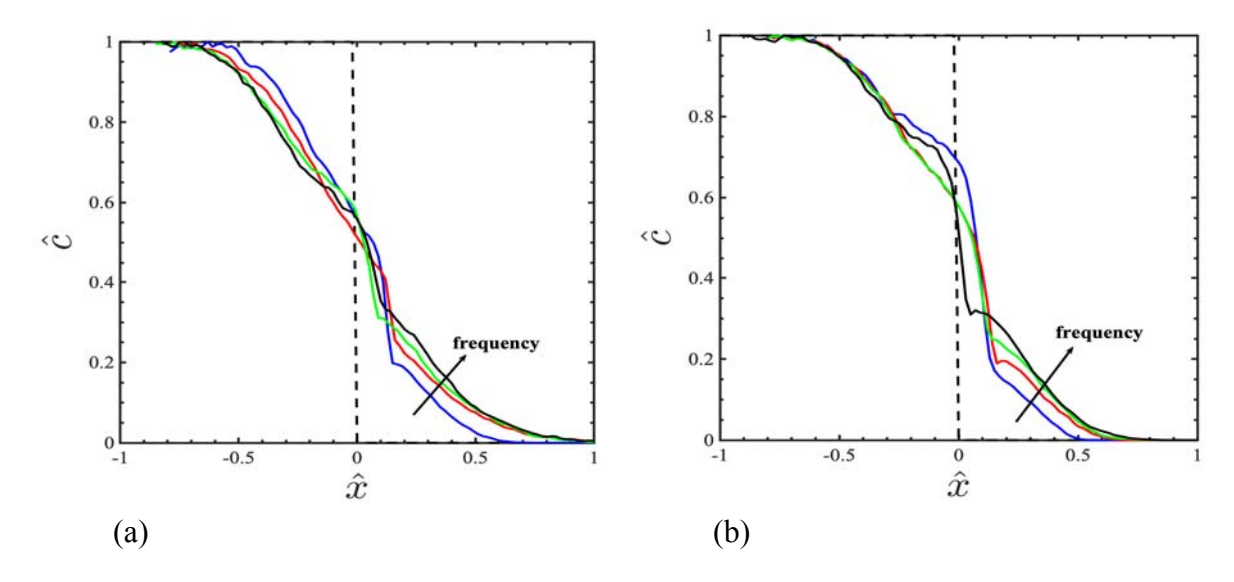


Figure 5. (Color online) Plots of normalized particle concentration for (a) 20 nm diameter particles and (b) 40nm particles measured at 45 min after hydrogel formation for the control case (blue) and cases treated with ultrasound of amplitude of 0.10 MPa of frequency 0.50 MHz (red), 1.00 MHz (black) and 2.25 MHz (green). The arrow shows the direction of increasing frequency.

The effect of ultrasound exposure time on the particle diffusion was examined by comparing results with 5 and 10 min exposure times and different ultrasound frequencies, in both cases with a 10% duty cycle. An example case with 1.0 MHz frequency and 0.1 MPa amplitude is shown in Figure 6 for 20 and 40 nm. For the 20 nm particles, we observe a significant enhancement of particle diffusion between the control case and the case with 5 min ultrasound exposure, and then a smaller increase in particle diffusion for the case with 10 min exposure. The 40 nm particles exhibit a similar trend, but with an overall slower diffusion rate.

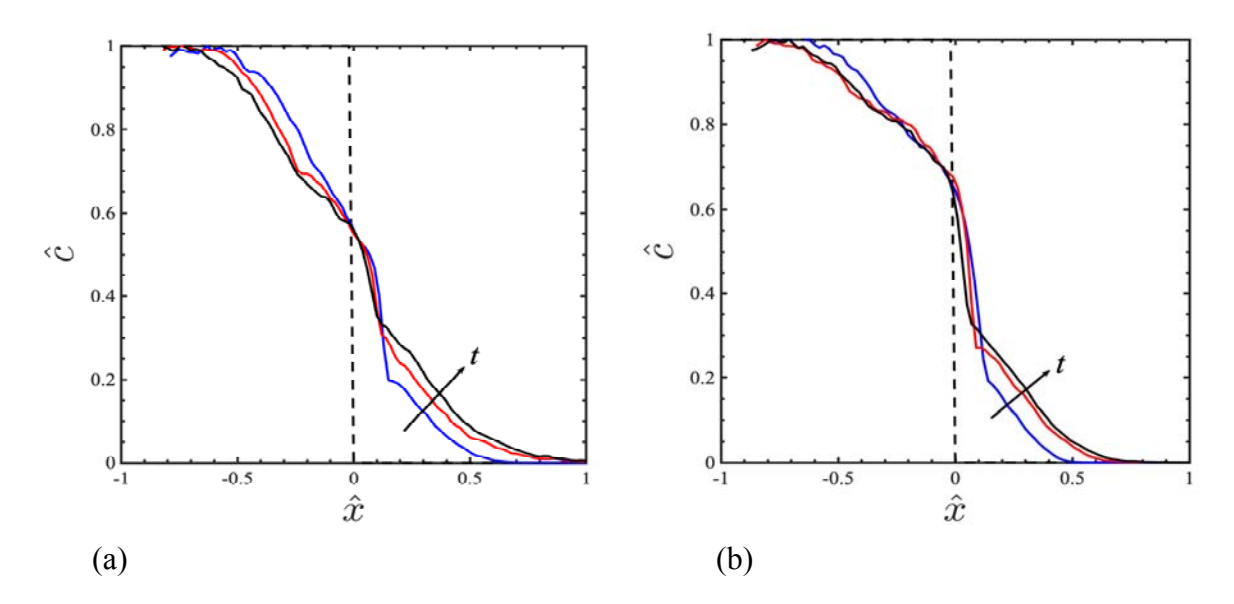


Figure 6. (Color online) Plots of normalized particle concentration for (a) 20 nm diameter particles and (b) 40nm particles measured at 45 min after hydrogel formation for the control case (blue) and cases treated with ultrasound of amplitude of 0.10 MPa of frequency 1.00 MHz for 5 min exposure (red) and for 10 min exposure (black). The arrow shows the direction of increasing exposure time (t).

IV. DISCUSSION

In this section, the diffusion coefficient D is estimated for each experimental case by determining the value of D for which solution of the one-dimensional diffusion equation yields the best fit to the observed data at 45 min after hydrogel formation. It was assumed that the diffusion coefficient due to Brownian motion (D_M , molecular diffusion) and that due to the ultrasound forcing (D_A , oscillatory diffusion) are additive to obtain the total diffusion coefficient.

The concentration for the control samples (with no ultrasound treatment) is governed by the standard diffusion equation

312
$$\frac{\partial c}{\partial t} = D_M \frac{\partial^2 c}{\partial x^2} \qquad \text{for } 0 \le t \le t_f,$$
 (7)

where t is time since formation of the hydrogel, x is depth within the unseeded agarose hydrogel film, and t_f is the time interval following hydrogel formation at which the images were obtained. The initial particle concentration was assumed to be given by $c(x,0) = c_0[1-U(x)]$, where U(x) is the step function. The final value of c(x,t) at time t_f for the control sample is denoted by $C_C(x) \equiv c(x,t_f)$.

When a sample is treated with ultrasound, the enhanced particle concentration exhibits additional diffusion, given by

322
$$\frac{\partial c}{\partial \tau} = D_A \frac{\partial^2 c}{\partial x^2} \qquad \text{for } 0 \le \tau \le t_A, \tag{8}$$

where t_A is the time duration of ultrasound application and τ is a pseudo time variable. Equation (8) was solved numerically with the initial condition $c(x, \tau = 0) = C_C(x)$, and the final value of the concentration obtained from solution of (8) at $\tau = t_A$ is denoted by $C_T(x) \equiv c(x, \tau = t_A)$.

Numerical solution of (7) and (8) was performed using the Crank-Nicholson method with time and spatial steps sizes $\Delta t/T=0.001$ and $\Delta x/L=0.01$, where T and L are characteristic time and length scales of the computation. The experimental data for the control and treated normalized concentration fields measured at the imaging time t_f are denoted by $e_C(x)$ and $e_T(x)$, respectively. Least-square error measures E_C and E_T are defined by

333
$$E_C = \int_0^L [e_C(x) - C_C(x)]^2 dx, \qquad E_T = \int_0^L [e_T(x) - C_T(x)]^2 dx. \qquad (9)$$

The numerical solution of (7) and (8) was repeated for a range of values of D_M and D_A , and the corresponding error measures from (9) were tabulated for each case. The optimal diffusion coefficient values were set equal to the values with the smallest least-square error values.

An example comparing the best-fit diffusion curves with the binned experimental data is given in Figure 7 for 20 nm diameter particles. We observe that away from the origin, the computed diffusion curves fit reasonably well with the experimental data. Very close to the origin, the experimental data exhibits a jump that is not observed in the computed diffusion curves. This jump in the experimental data is believed to be due to the impedance of the interface between the two layers on passage of particles from one layer to the other.



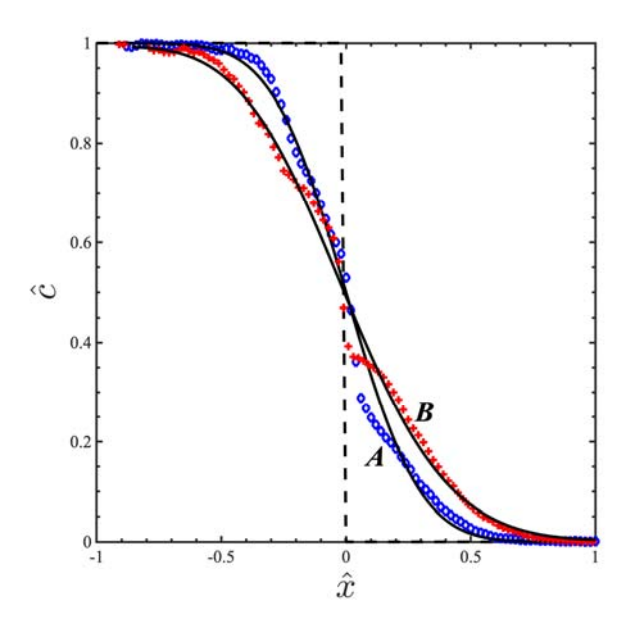


Figure 7. (Color online) Plot of the normalized particle concentration for 20 nm diameter particles measured at 45 min after hydrogel formation, showing binned experimental data (symbols) and best-fit diffusion predictions (black curves) for the control case (A, blue) and a case treated with ultrasound of amplitude 0.18 MPa at 1.0 MHz frequency (B, red).

An analytical prediction for the acoustic diffusion coefficient in oscillatory diffusion processes was given by Balakrishnan and Venkataraman (1981) using a two-time continuous

time random walk (CTRW) theory, in which particles are assumed to randomly flip between an oscillating state and a state in which they move at a constant random walk velocity. The resulting formula for the acoustic diffusion coefficient can be written as

357
$$D_{A} = \frac{A_{part}^{2}}{2\tau_{0}} \left[\frac{4\pi^{2}\tau_{0}^{2}f^{2}}{1 + 4\pi^{2}\tau_{0}^{2}f^{2}} \right]. \tag{10}$$

In this equation, f is the ultrasound frequency and A_{part} is the amplitude of non-hindered particle oscillation in the porous medium. Under conditions of linear acoustics, it is expected that A_{part} is proportional to the ultrasound amplitude A. The parameter τ_0 denotes the average particle holding time in the oscillating state, in-between particle capture events. The CTRW theory assumes that the particle holding time has an exponential distribution for both the captured state and the oscillating state.

The acoustic diffusion coefficient D_A was estimated from the binned experimental data for each case examined. All results reported in the paper were obtained as the average value of diffusion coefficient from repeated experiments with three different hydrogels. The estimated acoustic diffusion coefficient D_A is plotted as a function of ultrasound amplitude in Figure 8a at a frequency of f=1.0 MHz and as a function of frequency in Figure 8b at an amplitude of A=0.1 MPA, for both 20 nm and 40 nm diameter particle sizes. The error bars in Figure 8a were determined for each case by the root-mean-square of the acoustic diffusion coefficient values for repeated tests with three different hydrogels. The measured average value of the molecular diffusion coefficient D_M for these hydrogels were 6.31 μ m²/s and 3.29 μ m²/s for 20nm and 40nm diameter particles, respectively. The curves shown in Figure 8a were generated

by fitting a quadratic equation of the form $D_A = cA^2$, where c is a fitting coefficient, to the estimated acoustic diffusion coefficient values for the $f = 1.0 \, \mathrm{MHz}$ data. The form of this curve is motivated by the dependence of D_A on A_{part} in (10), and the assumption that A_{part} is linearly proportional to the ultrasound amplitude A. This expression is observed to be a reasonably good fit to the acoustic diffusion coefficient values, indicating that the dependence on amplitude indicated by the theoretical expression (10) is consistent with our experimental data.

The dependence of acoustic diffusion coefficient with frequency is examined in Figure 8b. The open symbols in this figure are based on an ultrasound exposure time of 5 min, and the filled symbols are based on an ultrasound exposure time of 10 min. Consistent with Figure 5, we observe a modest increase in the acoustic diffusion coefficient with increase in ultrasound frequency and with increase in the acoustic exposure time. In order to compare this data to the theoretical result (10) for the acoustic diffusion coefficient, we fit curves of the form $D_A = C_1 f^2 / (1 + C_2 f^2)$ to the data for each particle size. In both cases the best-fit curves yield the same value of the coefficient C_2 , which from (10) corresponds to an average particle hold-up time of $\tau_0 \cong 0.41~\mu s$. Our results therefore provide strong confirmation of both the amplitude and frequency dependence in the theoretical prediction (10) for acoustic-enhance nanoparticle diffusion in a hydrogel.

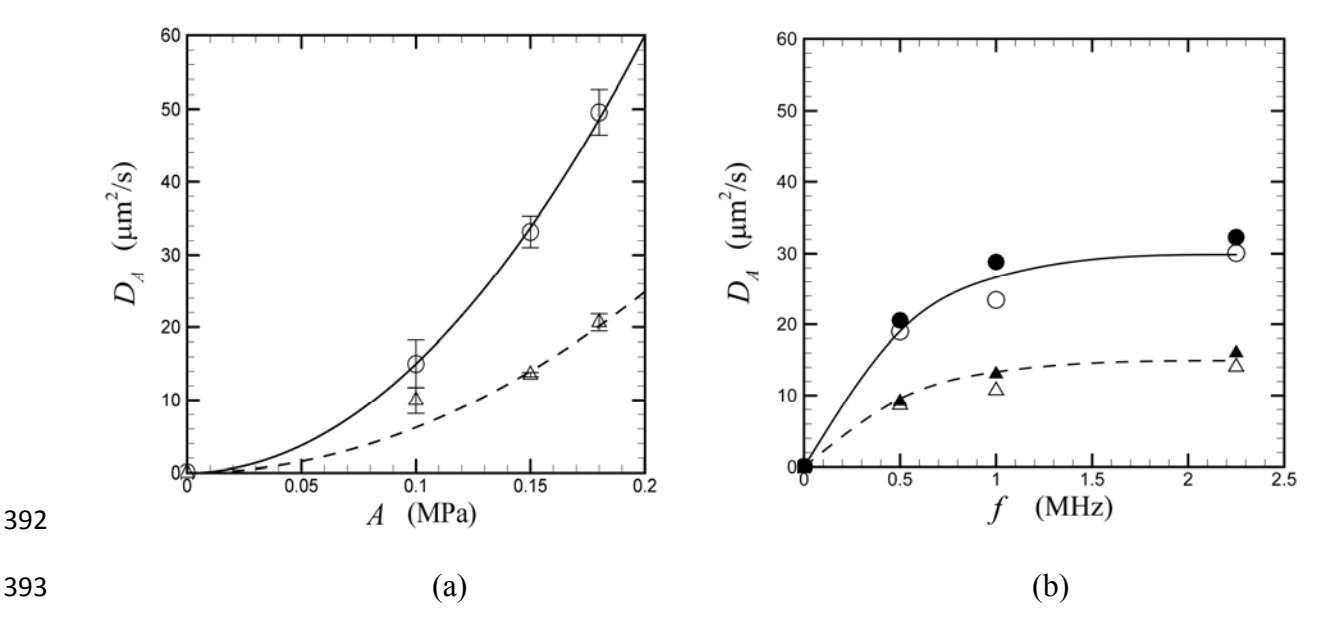


Figure 8. Acoustic diffusion coefficient D_A as a function of (a) ultrasound amplitude A at a frequency of 1.0 MHz and (b) ultrasound frequency f at an amplitude of 0.1 MPa. Data is shown for 20 nm diameter particles (circles) and 40 nm diameter particles (triangles). The curves in (a) are quadratic functions of the form $D_A = cA^2$ and the curves in (b) are functions of the form $D_A = C_1 f^2 / (1 + C_2 f^2)$, fit to the data for 20 nm particles (solid curve) and 40 nm particles (dashed curve). The open symbols are for data obtained after a 5 min ultrasound exposure time, and the filled symbols in (b) are for data obtained after a 10 min exposure time.

The integral penetration measure P provides a measure of the transport of particles from the seeded layer into the unseeded layer, starting with a value P=0 at the initial time and eventually approaching a value P=0.5 as the system approaches the equilibrium state in which the concentration achieves a uniform value across both layers. The values of the integral penetration measure P for different cases with 20 nm and 40 nm diameter particles examined at 45 min after hydrogel formation are plotted in Figure 9 as a function of ultrasound amplitude A at a frequency of 1.0 MHz (Figure 9a) and ultrasound frequency f at an amplitude of 0.1 MPa (Figure 9b). The values plotted were obtained from the average value for the three hydrogels tested for each case. For the control case (f = A = 0), the diffusion process is purely molecular, whereas for the ultrasound-treated cases, both molecular diffusion and acoustic diffusion

contribute to the measured values of *P*. In Figure 9a, the measured values of *P* obtained from binned experimental values are indicated by symbols and curves are fit to the predicted values from the fit diffusion solutions. Figure 9a indicates an increased penetration of particles into the initially unseeded layer with increase in ultrasound amplitude. Figure 9b similarly indicates an increase in the penetration of particles into the unseeded layer with increase in the ultrasound frequency. As expected, the case with 10 min exposure time (denoted by filled symbols in Figure 9b) exhibited increased particle penetration into the unseeded layer compared to cases with 5 min exposure time (denoted by open symbols).



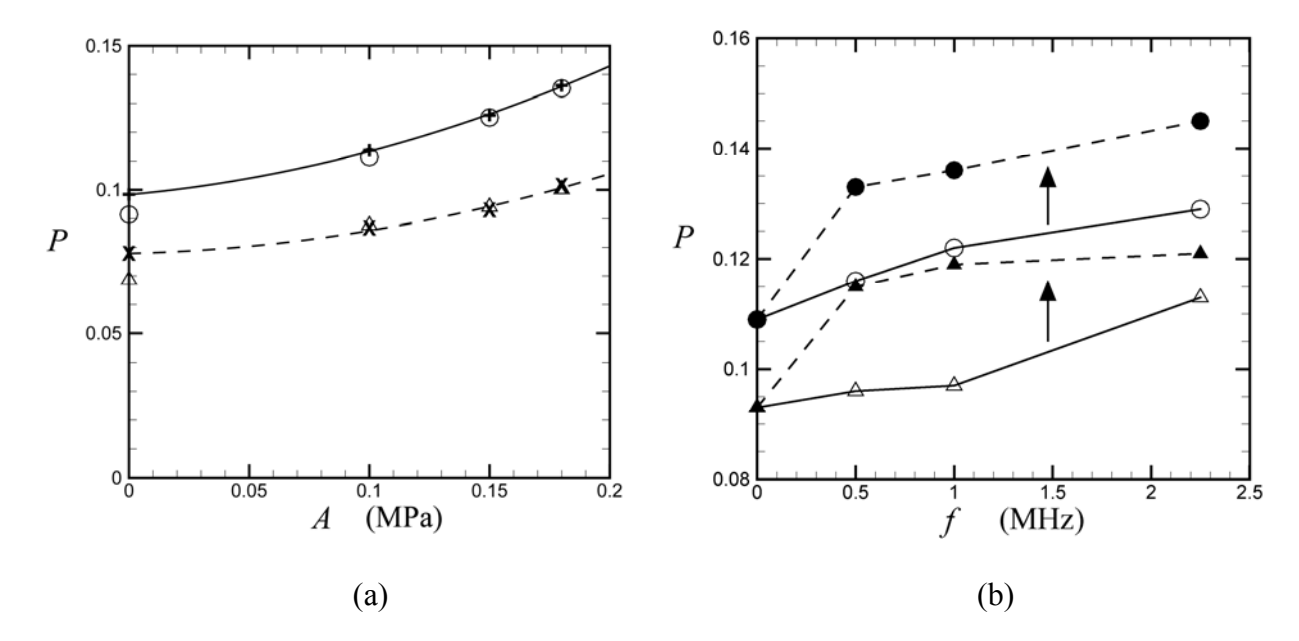


Figure 9. Plots of the integral penetration measure P for 20nm particles (circles) and 40 nm particles (triangles) as a function of (a) ultrasound amplitude A at a frequency of 1.0 MHz and (b) ultrasound frequency f at an amplitude of 0.1 MPa at a time of 45 min after hydrogel formation. In (a), predicted values obtained from the diffusion equation solutions are denoted by a '+' for the 20 nm particles and by a 'X' for the 40 nm particles. The solid and dashed curves are best quadratic fits to the computed diffusion curve values for the 20 nm and 40 nm particles, respectively. In (b), the data is given for ultrasound exposures of both 5 min (open symbols) and 10 min (filled symbols).

We note that it cannot be entirely excluded that the ultrasound damaged the hydrogel and that this could have influenced the data to some extent. We took precautions in conducting the experiments to avoid such damage, and we have good reasons to believe that damage either did not occur, or if it did that it was so minor as to have negligible effect on our conclusions. To avoid any possible damage, we were careful to select experimental conditions that minimized heating of the hydrogel. This is the reason that all tests were conducted with low ultrasound intensity at a 10% duty cycle, and for ultrasound exposure time periods of only 5 or 10 min. A demonstration that the ultrasound at these conditions did not influence the nanoparticle diffusion within the hydrogel is given in Figure 8b, where diffusion coefficient values are presented as a function of frequency for both 5 and 10 min ultrasound exposures. The diffusion coefficients obtained with these two exposure times are close to each other, as would be expected if there were no effect on the hydrogel from the ultrasound.

We conducted a test of diffusion coefficient following ultrasound exposure for ultrasound treated samples prepared as described in Section II, with 5 min ultrasound exposure period, 1.0 MHz frequency and 0.1 MPa amplitude ultrasound, and 20 nm particles. After the ultrasound was turned off, we continued to monitor the fluorescence field at 10 min intervals out to a time of 75 min. Using a sample of the same hydrogel, we also conducted a control experiment out to a time of 75 min with no ultrasound. The control experiment was used to determine the molecular diffusion coefficient, as described in Section IV. The acoustic diffusion coefficient obtained in these experiments was $D_A = 16.6 \pm 0.8 \,\mu\text{m}^2/\text{s}$, which is in the uncertainty range of the value given under the stated conditions in Figure 8a ($D_A = 15.0 \pm 3 \,\mu\text{m}^2/\text{s}$). The molecular diffusion coefficient was measured after the ultrasound was turned off at 55, 65 and 75 min, and the values obtained were found to be within the uncertainty range of the values for the control experiment.

The finding that the molecular diffusion coefficient after the ultrasound was turned off in the treated experiment returned to approximately the same value as for the control experiment supports our claim that the ultrasound did not damage the hydrogel.

Finally, we validated our experimental results for acoustic diffusion coefficient by showing that the measured values are in agreement with the theoretical predictions of Balakrishnan and Venkataraman (1981), as shown in Figure 8. If the hydrogel had been damaged by the ultrasound, we would expect a strong deviation from the theoretical $D_A = cA^2$ dependence predicted by Balakrishnan and Venkataraman (1981) for the high amplitude cases. Such deviation is not observed in our data shown in Figure 8a.

V. CONCLUSIONS

The effect of ultrasound on diffusion enhancement via the mechanism of oscillatory diffusion was examined for nanoparticles of different diameters in a two-layer agarose hydrogel for a range of different ultrasound amplitudes and frequencies. One layer of the hydrogel was initially seeded with fluorescent nanoparticles and the other layer was unseeded. The ultrasound was directed orthogonally to the layer surface, and it was run at a 10% duty cycle for both 5 and 10 min exposure times. The effective molecular and acoustic diffusion coefficients were estimated for each case by numerical solution of the diffusion equation and selecting the coefficient that yields the lowest value of the least-square error.

Molecular diffusion experiments were initially conducted with 20, 40, and 100 nm diameter nanoparticles. The 100 nm particles exhibited little diffusion, so the tests with ultrasound were conducted primarily with 20 and 40 nm particles. The 20 nm particles exhibited more rapid diffusion than the 40 nm particles for all cases examined. The effective diffusion

coefficient, which is composed of the sum of the molecular part D_M and the acoustic part D_A , was observed to increase significantly with increase in ultrasound amplitude. Effective diffusion coefficient values for the highest amplitude case examined, with $A=0.18\,$ MPa, were nearly an order of magnitude higher than the molecular diffusion coefficient for both particle sizes. The diffusion coefficient was also observed to increase modestly with the ultrasound frequency, with the acoustic diffusion coefficient increasing by about 50% for both particle sizes as the ultrasound frequency is increased from 0.5 MHz to 2.25 MHz. A measure of particle penetration from the seeded layer into the unseeded layer was also computed.

The trend in the estimated acoustic diffusion coefficient as a function of both ultrasound amplitude and frequency were found to compare closely with a theoretical prediction derived using the continuous time random walk (CTRW) theory for oscillating diffusion by Balakrishnan and Venkataraman (1981). This agreement is somewhat surprising, as the CTRW theory employs the highly simplified assumption that particles must occupy one of two states -- either oscillating freely in the porous medium or held captured within the medium. We note that a recent stochastic model by Curran and Marshall (2021) also demonstrated strong agreement with the CTRW prediction for acoustic diffusion coefficient. Both the current experimental finding and our previous computational finding provide confidence in our interpretation of the observed diffusion phenomenon.

The results of this study demonstrate that even low intensity ultrasound at a low duty cycle can be used to significantly enhance the rate of particle diffusion and penetration into a porous medium, such as a biofilm or human tissue. Nanoparticles have been effectively used for biofilm mitigation and for treatment of tumors in diseased tissue, but in most previous applications it was necessary that particles be magnetic so that they could be pulled into the

porous medium by a magnetic field. This requirement can make particle dispersal difficult and significantly limits particle selection. The results of the current paper suggest that exposure to low intensity pulsed ultrasound can be an effective method for controlling penetration of non-magnetic particles for treatment and/or mitigation of media such as biofilms or diseased tissue.

ACKNOWLEDGEMENTS

The authors wish to thank Prof. Matthew Wargo for useful discussions during this research and Nicole Bouffard for help with the confocal microscopy analysis at the Microscopy Imaging Center at the University of Vermont. This work was supported by the National Science Foundation under grant number CBET-1926197.

REFERENCES

Balakrishnan, V., and Venkataraman, G. (1981). "Two-state random walk model of diffusion. 2. Oscillatory diffusion," Pramana **16**(6), 437-455.

Beissner, K. (1987). "Radiation force calculations," Acta Acustica United with Acustica **62**, 255-263.

Characklis, W.G. (1981). "Bioengineering report: Fouling biofilm development: A process analysis," *Biotechnol. Bioeng.* **23**, 1923-1960.

Cheow, W.S., Chang, M.W., and Hadinoto, K. (2011). "The roles of lipid in anti-biofilm efficacy of lipid-polymer hybrid nanoparticles encapsulating antibiotics," Colloids and Surfaces A: Physicochemical and Engineering Aspects **389**, 158-165.

Costerton, J.W., Stewart, P.S., and Greenberg, E.P. (1999). "Bacterial biofilms: A common cause of persistent infections," *Science* **284**, 1318-1322.

Curran, K., and Marshall, J.S. (2021). "Stochastic model of oscillatory diffusion for colloidal particles in a fixed porous bed," Chemical Engineering Science **246**, 116993.

Dan-Asabe, B., Yaro, S.A., Yawas, D.S., and Aku, S.Y. (2013). Water displacement and bulk density-relation methods of finding density of powdered materials," International Journal of Innovative Research in Science, Engineering and Technology **2**, 5561-5566.

Fatin-Rouge, N., Starchev, K., and Buffle, J. (2004). "Size effects on diffusion processes within agarose gels," Biophysical Journal **86**, 2710–2719.

Forier, K., Raemdonck, K., De Smedt, S.C., Demeester, J., Coenye, T., and Braeckmans, K. (2014). "Lipid and polymer nanoparticles for drug delivery to bacterial biofilms," Journal of Controlled Release **190**, 607-623 (2014).

Galvão, C.N., Sanches, L.M., Mathiazzi, B.I., Ribeiro, R.T., Petri, D.F.S., and Carmona-Ribeiro, A.M. (2018). "Antimicrobial coatings from hybrid nanoparticles of biocompatible and antimicrobial polymers," International Journal of Molecular Sciences **19**(10), 2965. (doi: 10.3390/ijms19102965)

Han, C.D., Romero, N., Fischer, S., Dookran, J., Berger, A., and Doiron, A.L. (2017). "Recent developments in the use of nanoparticles for treatment of biofilms," Nanotechnology Reviews **6**, 383-404. (doi:10.1515/ntrev-2016-0054)

Jung, Y.-G., Choi, J., Kim, S.-K., Lee, J.-H., and Kwon, S. (2015). "Embedded biofilms, a new biofilm model based on the embedded growth of bacteria," Applied and Environmental Microbiology **81**(1), 211-219.

King, L.V. (1934). "On the acoustic radiation pressure of spheres," Proceedings of the Royal Society of London A **147**(861), 212-240.

Li, J., Nickel, R., Wu, J., Lin, F., van Lierop, J., and Liu, S. (2019). "A new tool to attack biofilms: driving magnetic iron-oxide nanoparticles to disrupt the matrix," Nanoscale **11**(14), 6905-6915. (doi:10.1039/C8NR09802F)

Li, L.-L., Yu, P., Wang, X., Yu, S.-S., Mathieu, J., Yu, H.-Q., and Alvarez, P.J.J. (2017). "Enhanced biofilm penetration for microbial control by polyvalent phages conjugated with magnetic colloidal nanoparticle clusters (CNCs)," Environmental Science: Nano 4, 1817-1826.

Ma, D., Green, A.M., Willsey, G.G., Marshall, J.S., Wargo, M.J., and Wu, J.R. (2015). "Effects of acoustic streaming from moderate-intensity pulsed ultrasound for enhancing biofilm mitigation effectiveness of drug-loaded liposomes," Journal of the Acoustical Society of America **138**(2), 1043-1051.

Ma, D., Marshall, J.S., and Wu, J.R. (2018). "Measurement of ultrasound-enhanced diffusion coefficient of nanoparticles in an agarose hydrogel," Journal of the Acoustical Society of America 114(6), 3496-3502.

Makris, K.C., Andra, S.S., and Botsaris, G. (2014). "Pipe scales and biofilms in drinking-water distribution systems: undermining finished water quality," Crit. Rev. Environ. Sci. Technol. 44, 1477-1523. (doi:10.1080/10643389.2013.790746)

Marshall, J.S. (2016). "A model of ultrasound-enhanced diffusion in a biofilm," Journal of the Acoustical Society of America **139**(6), EL228-EL233.

Marshall, J.S., Arnold, C., Curran, K., and Chivers, T. (2021). "Statistics of particle diffusion subject to oscillatory flow in a porous bed," Chemical Engineering Science **231**, 116239.

Millenbaugh, N.J., Baskin, J.B., DeSilva, M.N., Elliot, W.R., and Glickman, R.D. (2015). "Photothermal killing of *Staphylococcus aureus* using antibody-targeted gold nanoparticles," International Journal of Nanomedicine **10**, 1953–1960. (doi: 10.2147/IJN.S76150)

Mohammed, L., Gomaa, H.G., Ragab, D., and Zhu, J. (2017). "Magnetic nanoparticles for environmental and biomedical applications: A review," Particuology **30**, 1-14. (doi:https://doi.org/10.1016/j.partic.2016.06.001)

Peulen, T.-O., and Wilkinson, K.J. (2011). "Diffusion of nanoparticles in a biofilm," Environmental Science & Technology **45**, 3367-3373. (doi:10.1021/es103450g).

Rowley, J.A., Madlambayan, G., and Mooney, D.J. (1999). "Agarose hydrogels as synthetic extracellular matrix materials," Biomaterials **20**(1), 45-53.

Schroeder, A., Kost, J., and Barenholz, Y. (2009). "Ultrasound, liposomes, and drug delivery: principles for using ultrasound to control the release of drugs from liposomes," Chemistry and Physics of Lipids **162**, 1-16.

Shaw, G.J., Meunier, J.M., Huang, S.-L., Lindsell, C.J., McPherson, D.D., and Holland, C.K. (2009). "Ultrasound-enhanced thrombolysis with tPA-loaded echogenic liposomes," Thrombus Research **124**, 306-310.

Siddique, M.H., Aslam, B., Imran, M., Ashraf, A., Nadeem, H., Hayat, S., Khurshid, M., Afzal, M., Malik, I.R., Shahzad, M., Qureshi, U., Khan, Z.U.H., and Muzammil, S. (2020). "Effect of silver nanoparticles on biofilm formation and EPS production of multidrug-resistant *Klebsiella pneumoniae*," BioMed Research International **2020**, 6398165. (doi.org/10.1155/2020/6398165)

Singh, N.K., Wood, J.M., Karouia, F., and Venkateswaran, K. (2018). "Succession and persistence of microbial communities and antimicrobial resistance genes associated with International Space Station environmental surfaces," Microbiome **6**, 204. (doi:10.1186/s40168-018-0585-2)

Singh, S., Singh, S. K., Chowdhury, I., and Singh, R. (2017). "Understanding the mechanism of bacterial biofilms resistance to antimicrobial agents," Open Microbiolology Journal 11, 53-62. (doi:10.2174/1874285801711010053)

Smidsród, O., and Skjåk-Brik, G. (1990). "Agarose as immobilization matrix for cells," Trends in Biotechnology **8**, 71-78.

Thomas, J.M., and Chrysikopoulos, C.V. (2007). "Experimental investigation of acoustically enhanced colloid transport in water-saturated packed columns." Journal of Colloid and Interface Science **308**, 200-207.

Tiukinhoy-Laing, S.D., Huang, S., Klegerman, M., Holland, C.K., and McPherson, D.D. (2006). "Ultrasound-facilitated thrombolysis using tissue-plasminogen activator-loaded echogenic liposomes," Thrombosis Research **119**(7), 777-784.

Venkateswaran, K., La Duc, M.T., and Horneck, G. (2014). "Microbial existence in controlled habitats and their resistance to space conditions," Microbes and Environments **29**, 243-249. (doi:10.1264/jsme2.ME14032)

Vogler, T., and Chrysikopoulos, C.V. (2002). "Experimental investigation of acoustically enhanced solute transport in porous media," Geophysical Research Letters **29**(15), 1710.

Wu, J. (1996). "Determination of velocity and attenuation of shear waves using ultrasonic spectroscopy," The Journal of the Acoustical Society of America **99**(5), 2871-2875.

Zharov, V.P., Mercer, K.E., Galitovskaya, E.N., and Smeltzer, M.S. (2006). "Photothermal nanotherapeutics and nanodiagnostics for selective killing of bacteria targeted with gold nanoparticles," Biophysical Journal **90**, 619–627.

FIGURE CAPTIONS

Figure 1. (Color online) Experimental set-up for the ultrasound measurements.

Figure 2. (Color online) Images obtained from a confocal microscope for the agarose hydrogel seeded with 20nm particles for different ultrasound conditions after 45 minutes of hydrogel formation: (a) control (no ultrasound); (b) treated using 1 MHz, 0.10 MPa ultrasound waves; (c) treated using 1 MHz, 0.15 MPa ultrasound waves; (d) treated using 1 MHz, 0.18 MPa ultrasound

waves.

Figure 3. (Color online) Plots of particle normalized concentration \hat{c} as a function of dimensionless distance \hat{x} for control cases: (a) comparison at 45 min after hydrogel formation for particle diameters 20 nm (C, blue), 40 nm (B, red) and 100 nm (A, green); (b) plot for 20 nm particles at times after hydrogel formation of 10 min (blue), 20 min (red), 30 min (green) and 40 min (black). The standard deviation estimates lie within 0.01 for each condition. The arrow in (b)

shows the direction of increasing time (t).

Figure 4. (Color online) Plots of normalized particle concentration for (a) 20 nm diameter particles and (b) 40nm particles measured at 45 min after hydrogel formation for the control case (blue) and cases treated with ultrasound of amplitude 0.10 MPa (red), 0.15 MPa (green) and 0.18 MPa (black) at 1 MHz frequency. The arrow shows the direction of increasing amplitude (4)

MPa (black) at 1 MHz frequency. The arrow shows the direction of increasing amplitude (*A*).

Figure 5. (Color online) Plots of normalized particle concentration for (a) 20 nm diameter particles and (b) 40nm particles measured at 45 min after hydrogel formation for the control case

(blue) and cases treated with ultrasound of amplitude of 0.10 MPa of frequency 0.50 MHz (red), 1.00 MHz (black) and 2.25 MHz (green). The arrow shows the direction of increasing frequency.

Figure 6. (Color online) Plots of normalized particle concentration for (a) 20 nm diameter particles and (b) 40nm particles measured at 45 min after hydrogel formation for the control case (blue) and cases treated with ultrasound of amplitude of 0.10 MPa of frequency 1.00 MHz for 5 min exposure (red) and for 10 min exposure (black). The arrow shows the direction of increasing exposure time (*t*).

Figure 7. (Color online) Plot of the normalized particle concentration for 20 nm diameter particles measured at 45 min after hydrogel formation, showing binned experimental data (symbols) and best-fit diffusion predictions (black curves) for the control case (A, blue) and a case treated with ultrasound of amplitude 0.18 MPa at 1.0 MHz frequency (B, red).

Figure 8. Acoustic diffusion coefficient D_A as a function of (a) ultrasound amplitude A at a frequency of 1.0 MHz and (b) ultrasound frequency f at an amplitude of 0.1 MPa. Data is shown for 20 nm diameter particles (circles) and 40 nm diameter particles (triangles). The curves in (a) are quadratic functions of the form $D_A = CA^2$ fit to the data for 20 nm particles (solid curve) and 40 nm particles (dashed curve). The open symbols are for data obtained after a 5 min ultrasound exposure time, and the filled symbols in (b) are for data obtained after a 10 min exposure time.

Figure 9. Plots of the integral penetration measure P for 20nm particles (circles) and 40 nm particles (triangles) as a function of (a) ultrasound amplitude A at a frequency of 1.0 MHz and

(b) ultrasound frequency f at an amplitude of 0.1 MPa at a time of 45 min after hydrogel formation. In (a), predicted values obtained from the diffusion equation solutions are denoted by a '+' for the 20 nm particles and by a 'X' for the 40 nm particles. The solid and dashed curves are best quadratic fits to the computed diffusion curve values for the 20 nm and 40 nm particles, respectively. In (b), the data is given for ultrasound exposures of both 5 min (open symbols) and 10 min (filled symbols).